Superconductivity in thallium double atomic layer and transition into an insulating phase intermediated by a quantum metal state

2017 2D Mater. 4 025020

(http://iopscience.iop.org/2053-1583/4/2/025020)

2D Materials

CrossMark

RECEIVED
6 September 2016

REVISED
18 December 2016

ACCEPTED FOR PUBLICATION
9 January 2017

PUBLISHED
1 February 2017

PAPER

Superconductivity in thallium double atomic layer and transition into an insulating phase intermediated by a quantum metal state

S Ichinokura[1], L V Bondarenko[2,3], A Y Tupchaya[2,3], D V Gruznev[2,3], A V Zotov[2,3,4], A A Saranin[2,3] and S Hasegawa[1]

[1] Department of Physics, University of Tokyo, 7-3-1 Hongo, Bunkyo-ku, Tokyo 113-0033, Japan
[2] Institute of Automation and Control Processes FEB RAS, 690041 Vladivostok, Russia
[3] School of Natural Sciences, Far Eastern Federal University, 690000 Vladivostok, Russia
[4] Department of Electronics, Vladivostok State University of Economics and Service, 690600 Vladivostok, Russia

E-mail: ichinokura@surface.phys.s.u-tokyo.ac.jp

Keywords: bilayer thallium, surface analysis, two-dimensional superconductivity, quantum phase transition

Abstract

We report on the first observation of superconductivity in a double atomic layer of Tl on Si(1 1 1) using *in situ* electrical resistivity measurements in ultrahigh vacuum. The structure of the Tl bilayer was characterized by a set of techniques, including scanning tunneling microscopy, electron diffraction and photoemission spectroscopy, which confirmed the metastability and metallic nature of the Tl bilayer. The epitaxial growth of atomically thin 'soft' metallic film over the entire surface of substrate enabled us to find a macroscopic superconducting transition at 0.96 K, accompanied by thermal and quantum fluctuations of order parameter. The system also demonstrates a perpendicular-magnetic-field-induced superconductor-insulator transition, together with an intermediate metallic state. We have found that the magnetoresitivity at the lowest temperature is consistent with the Bose metal picture, which is a consequence of strong quantum fluctuations.

Introduction

Two-dimensional superconductivity (2DSC) has been studied for a long time. Early experimental demonstrations of 2DSC were performed in the late 1980s. First examples of superconductivity in ultrathin systems with few-monolayer thicknesses were quench-condensed films of Bi and Pb deposited on glazed alumina substrates coated with amorphous Ge [1]. In these systems, disorder- and magnetic-field-driven superconductor-insulator transitions (SITs) were intensively discussed in terms of quantum phase transition [2]. Thereafter, physics of 2DSC has been developed through the huge movement of high critical temperature (T_c) superconductors, which have layered quasi two-dimensional structures [3] and rise of the electric-field-induced 2DSC using ionic liquids [4, 5]. Great technical improvement of crystal growth has made it possible to fabricate various kinds of atomically clean 2D electron systems, leading to realization of thinner 2DSCs e.g. $LaAlO_3/SrTiO_3$ [6–8], Ga/GaN [9, 10], $FeSe/SrTiO_3$ [11], metal-doped graphenes [12, 13] and chalcogenide compounds [14, 15]. In these two-dimensional 'crystalline' superconductors, deeper insight into quantum phase transition has been suggested, such as intermediate Bose metal state [14] and quantum Griffiths singularity [8, 10]. These studies opened up a way to approach to bosonic systems: non-superfluid liquid of Cooper pairs or vortex glass phase. Because Bose–Einstein condensation has recently received much attention with lots of experiments reporting Bose superfluidity in optical lattices of alkali atoms [16, 17], it is a big challenge to establish bosonic ground states in condensed matter.

Another blanch of 2D crystalline superconductors is metallic overlayers on semiconductor surfaces. In particular, so-called metal-adsorbed surface reconstructions promise the single or double atomic layer 2DSC owing to their good wettability. In/Si(1 1 1) and Pb/Si(1 1 1) systems are the first examples of atomically thinned 2DSCs [18–20]. Thallium (Tl) layers on Si(1 1 1) seem to be promising systems because glass-supported Tl films with tens nm thickness show superconductivity at 2.4 K [21]. Adsorption of Tl, the heaviest Group III metal, onto Si(1 1 1) has already been found to present a set of fascinating phenomena. In particular, deposition of Tl submonolayers onto the Si(1 1 1)7 × 7 template results in formation of the ordered arrays of magic clusters [22–28]. Due to a variable valency, one or three, Tl induces the $\sqrt{3} \times \sqrt{3}$ reconstruction

[29, 30] like other Group III metals, but it induces also the 3×1 reconstruction [29, 31] akin to that typical for alkali metals. In addition, one monolayer of Tl forms a specific 1×1 reconstruction [23, 29, 32, 33] having a structure of a pseudomorphic layer where Tl atoms occupy every T_4 sites atop a bulk-truncated Si(1 1 1) surface [34–36]. The 1×1-Tl reconstruction has recently attracted a great attention due to a giant Rashba-type spin-splitting of its surface bands [37–43]. Further deposition of Tl onto the 1×1-Tl leads to the formation of the 'soft' Tl double layer region showing a 6×6 periodicity [32, 44]. However, its atomic arrangement and electronic properties still remain unknown and no one has performed epitaxial growth of the double layer in wafer scale with good reproducibility. Such well-defined double atomic layer film is ideal stage to investigate intrinsic two-dimensional transport phenomena. Note that stable double-layer structures are seldom and non-typical for metals on Si(1 1 1). Besides Tl/Si(1 1 1), the other known example is the so-called quasi-rectangular rec-$\sqrt{7} \times \sqrt{3}$-In phase on Si(1 1 1) surface with double In overlayer. [45–47]. Recent discovery of superconductivity in the latter phase [18–20] gives a promise for finding the same in the Tl double-layer film. An additional promise for Tl layers stems also from the found superconductivity in the monatomic-layer Tl compound with Pb on Si(1 1 1) [48].

In the present paper, we report on the first experimental demonstration of superconductivity in the Tl double layer on Si(1 1 1). First, we present a comprehensive structural analysis. We observed that the entire surface of substrate is covered by epitaxial 'soft' Tl metal overlayer showing a 6×6 periodicity, by depositing the second monolayer of Tl on Si(1 1 1)1×1-Tl (the first layer of Tl) surface at ambient temperature. *In situ* electron diffraction and photoemission measurements indicated that the Tl double layer is easily destroyed by excess Tl atoms deposition, which induces condensation into three-dimensional island structures. Angle-resolved photoemission spectroscopy revealed that this metastable bilayer is metallic, that is distinct from the pristine Tl monolayer, an insulating 1×1-Tl phase. Detection of superconductivity was done by *in situ* four-point probe (4PP) electric resistance measurements in ultrahigh vacuum (UHV), showing a transition temperature of 0.96 K. By applying perpendicular magnetic field, we found a superconductor-insulator transition, accompanied with an intermediate metallic state. This is a quantum-metallic state called 'Bose metal' in which Cooper pairs do not have global coherency. This complicated phase transition originates from the interplay among quenched disorder, thermal and phase fluctuations, as proposed in the long history of 2DSC.

Experimental details

Measurements were performed in two separate UHV systems. Scanning tunneling microscopy (STM), low-energy electron diffraction (LEED), core-level ultraviolet photoelectron spectroscopy (CLUPS) and angle-resolved photoelectron spectroscopy (ARPES) experiments were conducted in Omicron MULTIPROBE system. STM images were acquired in a constant-current mode with a mechanically cut PtIr tip after annealing in vacuum. ARPES measurements were conducted using VG Scienta R3000 electron analyzer and high-flux He discharge lamp with toroidal-grating monochromator as a light source. The *in situ* electronic resistivity measurements were performed with a UHV-4PP system, where a 4PP consisting of four copper wires with 100 μm diameter was attached to the STM head, where the sample and 4PP were cooled down to 0.8 K and a magnetic field up to 7 T was applied perpendicular to the surface. The sheet resistivity R_{sheet} was obtained by the 4PP dc current–voltage measurement, by using the dual configuration method to avoid data scattering due to the error in probe spacing. The apparatus was also equipped with reflection high-energy electron diffraction (RHEED) for sample characterization with deposition [49].

Atomically-clean Si(1 1 1)-7×7 surfaces were prepared *in situ* by repeated flashing the samples to 1280 °C. Si(1 1 1)-1×1-Tl reconstruction was prepared by depositing 1 ML Tl from a Ta-tube effusion cell onto Si(1 1 1)-7×7 surface held at $\sim$300 °C (1 ML (monolayer) $= 7.8 \times 10^{14}$ cm^{-2}).

Results and discussion

Tl double layer formation

Formation of the double-layer Tl phase takes place when Tl is deposited onto the Si(1 1 1)-1×1-Tl surface. In previous studies [32, 44], the substrates were kept at $\sim$ 300°C during deposition of the second Tl layer. At such high temperature, Tl bilayer grew as just a local structure. Here we found that deposition at lower temperatures ranging from room temperature (RT) to about 200 °C is essential to fabricate the bilayer structure homogeneously on the entire surface as described below. The second Tl layer starts preferentially from the atomic steps and spreads over terraces with growing Tl coverage. In large-scale STM images it appears as bright regions (figure 1(a)). Interestingly, the apparent height of the double-layer phase almost coincides with that of the 1×1-Tl phase on the upper terrace as illustrated in the inset in figure 1(a). In the middle-scale STM images, the double-layer Tl phase demonstrates a 6×6 periodicity. High-resolution STM observations reveal that the periodic structure is associated with developing of the moiré pattern within the array which preserves basic 1×1 periodicity (figure 1(c)). The double-layer 6×6-Tl phase is completed when somewhat more than 1 ML Tl is added on the 1×1-Tl surface. However, any Tl overdeposition (i.e. deposition of additional Tl onto the completed 6×6-Tl phase) destabilizes the Tl second layer which disintegrates into 3D islands restoring the 1-ML1×1-Tl structure on the baring surface. Our STM results are consistent with those reported by Vitali *et al*

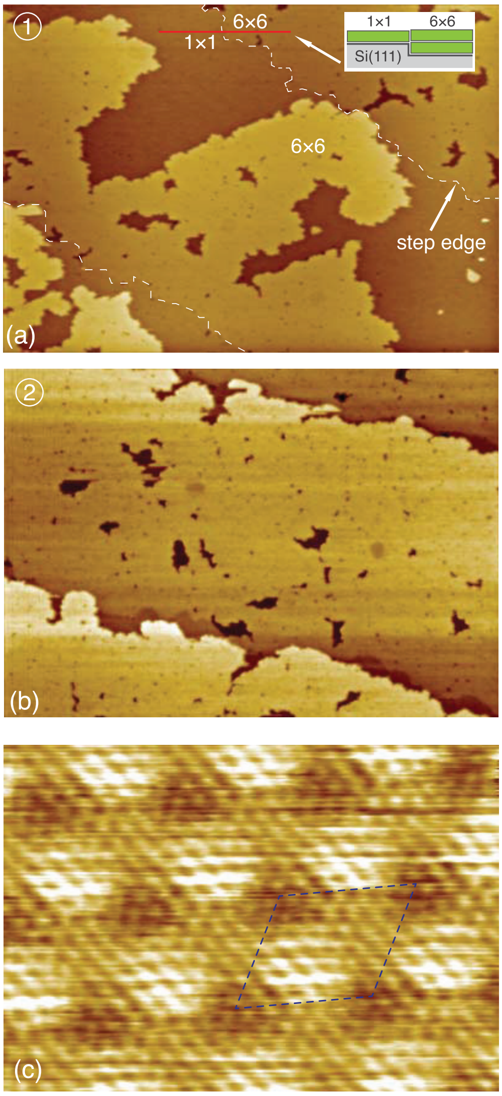

Figure 1. Large-scale (800×600 nm^2) STM images showing (a) intermediate and (b) final stages of the formation of the 6×6-Tl double-layer phase upon Tl deposition onto Si(1 1 1)-1×1-Tl surface held at 200 °C. Inset in (a) shows a schematic diagram of the Tl atomic layers on Si(1 1 1) along the red line in STM image crossing an atomic step (marked by dashed white line). (c) High-resolution (10×7.5 nm^2) STM image showing moiré structure of the Tl double layer. The 6×6 unit cell is outlined by a blue dashed line.

[44] who picked up the locally formed Tl double-layer phase on Si(1 1 1) by STM/S and considered such kind of instability as a sign of its structural 'softness'.

The STM-derived conclusions on the growth and decay of the Tl double layer find a clear confirmation in the results obtained with the diffraction techniques, LEED and RHEED (figure 2), and electron spectroscopy techniques, CLUPS and ARPES (figure 3). In particular, 6×6 extra-reflections appear in the LEED pattern around the main 1×1 spots as a result of Tl deposition (figure 2(a)). Note that occurrence of the extra-spots only in the vicinity of the main spots is a typical sign of the incommensurate structures. The extra-reflections become most intense when the 6×6-Tl double layer is completed and then they vanish with adding extra Tl (figure 2(b)). Since the 1×1 LEED pattern reflects the three-fold symmetry of the Si(1 1 1) surface, three fundamental spots out of six are brighter than the other three (figure 2(a)). The bright spots appear to be the most sensitive to the completion of the double-layer 6×6-Tl phase displaying the sharp minimum in their intensity as a function of Tl coverage in contrast to the less bright fundamental spots which show a shallow and broad minimum (figure 2(b)). RHEED results (figure 2(c)) are fully consistent with the LEED data. In addition, RHEED reveals formation of the 3D Tl islands after decay of the Tl double-layer phase. It should be noted, however, that some tailings of the 6×6 structure remain as evidenced by the faint 6×6 reflection remainders.

Evolution of the surface electronic properties during structural transformations in the course of Tl deposition is reflected in the electron spectroscopy results. In particular, as shown in figure 3(a), CLUPS reveals the 0.4 eV shift of Tl 5d peaks towards the lower binding energy upon the single-to-double layer transition after which Tl-to-Tl binding dominates over Tl-to-Si binding. When the double layer collapses after deposition of $\sim$3 ML Tl, the peaks become split, revealing coexistence of two types of Tl binding geometries, Tl-to-Tl and Tl-to-Si.

The ARPES data are presented in the form of the spectra along the $\overline{\Gamma}$-$\overline{K}$ direction and Fermi surface maps as shown in figures 3(b) and (c). In agreement with the previously reported data [37–43], the initial 1×1-Tl surface shows up basically as a semiconductor if one does not take into account the shallow pockets around the $\overline{K}$ points whose electron filling is associated with extra Tl atoms on the 1×1-Tl surface [39] in the form of specific surface defects [33]. With formation of the 6×6 Tl double layer, a distinct metallic surface-state band develops. In the Fermi surface map, it shows up as the inner contour having a shape of a concave hexagon. This contour is apparently a result of folding the large, bright, and almost circular contour located in the second 1×1 surface Brillouin zones (SBZs) into the first SBZ. There are also less distinct contours around the above mentioned one. But they are believed to be replica contours. They are not related to the real electron band structure of the Tl double layer, but result from interference of the ejected photoelectrons with the periodic potential of the moiré structure at the surface. The signs that these are replica bands are almost the same velocity of all the bands when crossing the Fermi level and absense of minigaps at the replicas crossing points. ARPES data on the overdeposition of Tl are in agreement with data of other techniques, namely, the surface displays the distinct features of the 1×1-Tl surface and those of the 6×6 structure remainders.

Transport properties of Tl double layer

Figures 4(a) and (b) show temperature dependent sheet resistivities $R_{\text{sheet}}(T)$ of the 1×1- and 6×6-Tl, respectively. The 1×1-Tl becomes insulating immediately after cooling from RT, as seen in figure 4(a).

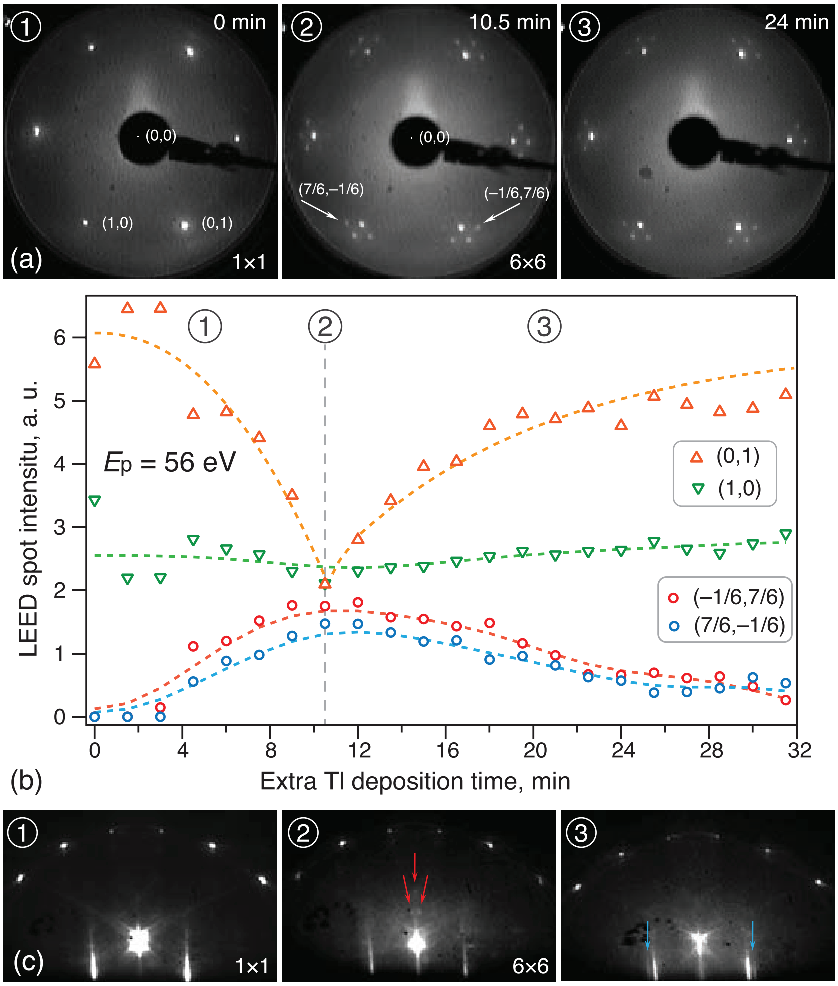

Figure 2. Diffraction data on the structural transformations on the surface upon Tl adsorption onto Si(1 1 1)-1 × 1-Tl surface. (a) LEED patterns and (b) dependence of intensity of LEED reflections indicated in (a) versus Tl dose. ①, ② and ③ denote the 6 × 6-Tl growth stages corresponding to the underdeposition, exact deposition and overdeposition of Tl, respectively. (c) RHEED patterns taken at the respective stages. Red arrows in ② indicate the 1/6-order reflections, blue arrows in ③ the reflections from 3D Tl islands.

This is in consistent with the previous reports by ARPES, suggesting its insulating band structure [37, 39, 40]. On the other hand, on the surface with the 6 × 6-Tl, R_{sheet} kept ca. 7.6 kΩ, well below the quantized resistance for electrons, $h/e^2 = 25.8$ kΩ (figure 4(b)). This indicates the metallic nature of the Tl double layer [22, 23]. One can see the most significant feature of this system, a superconducting transition below 1 K. The midpoint of resistance drop gives T_c ~0.96 K. The resistivity starts to decrease gradually below 4 K, which can be interpreted as an effect of amplitude fluctuations of the superconducting order parameter, and suggests strong two-dimensional nature of the present superconducting system. The following equations well reproduce this behavior as proved by the coincidence of the experimental data with the appropriate fitting curve shown by the black solid line in figure 4(b).

$$R = \frac{1}{\sigma_0 + \sigma_{AL} + \sigma'}, \quad (1)$$

$$\sigma_{AL} = \frac{e^2}{16\hbar} \cdot \frac{T_c}{T - T_c}, \quad (2)$$

$$\sigma' = \alpha \frac{e^2}{h} \ln T \quad (3)$$

where σ_{AL} is called Aslamazov–Larkin term, which describes the parallel conduction due to thermally excited Cooper pairs [50]. The last term σ' includes all possible components giving ln T behavior: weak (anti) localization and electron–electron interaction in the diffusion channel. From the numerical fitting, we obtained $T_c = 0.804 \pm 0.001$ K and $\alpha = 0.170 \pm 0.003$.

Another important point in the transition due to fluctuations can be seen in the temperature range where the resistivity approaches zero with a 'tail'. The tail in the resistance drop can be explained in terms of Berezinskii–Kosterlitz–Thouless (BKT) transition (figure 4(b), inset), which realizes a zero resistance state driven by the binding of vortex-antivortex pairs, generated by phase fluctuations of the order parameter. To determine the BKT transition temperature, we used the Halperin–Nelson equation [51],

$$R \propto \exp\left[-2b\left(\frac{T_c - T_{BKT}}{T - T_{BKT}}\right)^{1/2}\right], \quad (4)$$

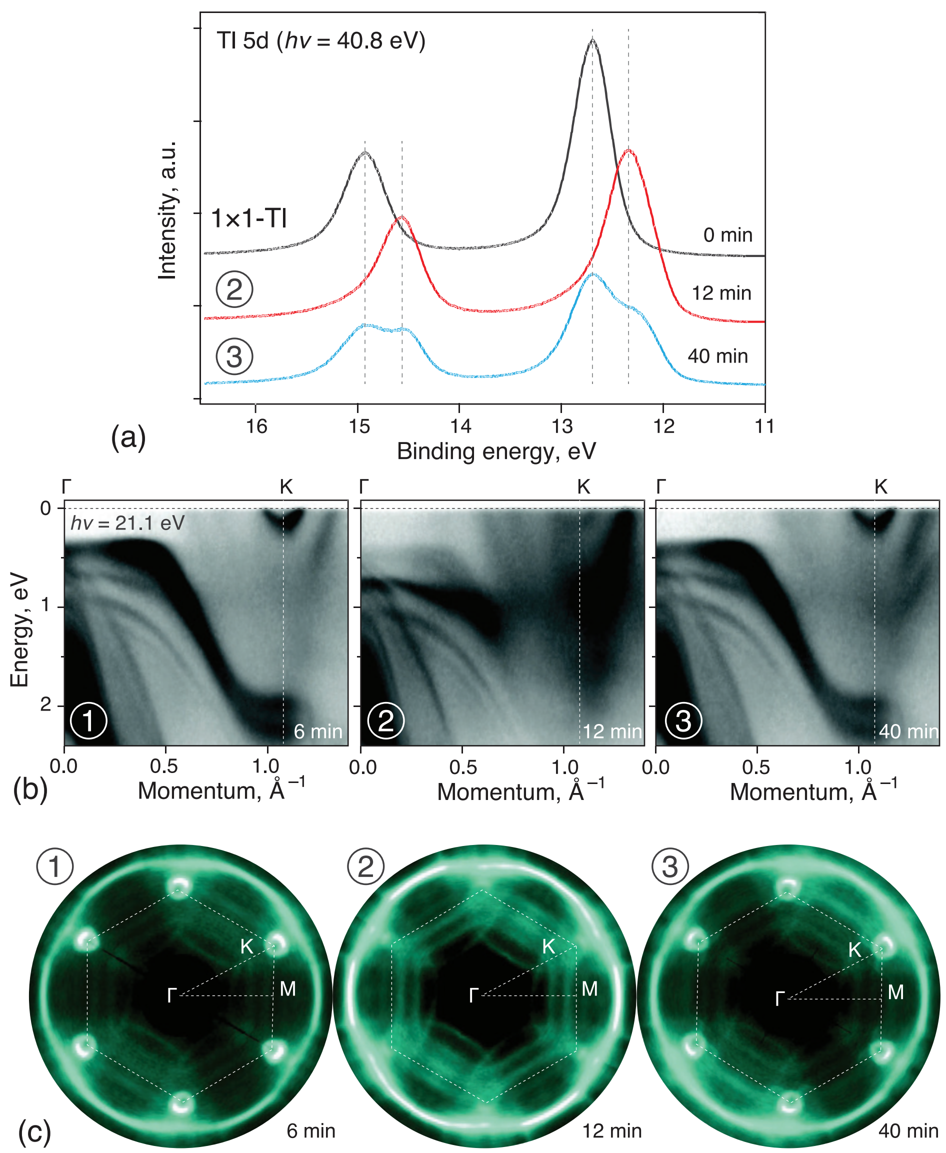

Figure 3. Electron spectroscopy data on the structural transformations on the surface upon Tl adsorption onto Tl/Si(1 1 1)1 × 1 surface. (a) CLUPS Tl 5d spectra taken from the initial 1 × 1-Tl surface (black line), completed 6 × 6-Tl double layer (red line) and Tl-overdeposited surface after decay of the Tl double layer (blue line). (b) ARPES spectra along the $\overline{\Gamma}$-$\overline{K}$ direction and (c) Fermi surface maps recorded from the surface at stages ①–③, i.e. after 6 min, 12 min and 40 min of Tl deposition, respectively, in figures 2(b) and (c).

where b is material dependent parameter. This shows a squareroot-cusp behavior that originates from the energy dissipation due to the vortex flow above the BKT transition temperature. The successful numerical fitting shown by the black dashed line in the inset suggests strong two-dimensionality of the present system and gives a superconducting and BKT transition temperatures $T_c = 1.0 \pm 0.3$ K and $T_{BKT} = 0.80 \pm 0.05$ K, respectively. The critical temperatures obtained from the fitting to equations (1) and (4) are consistent with the T_c of 0.96 K, estimated from the midpoint of resistance curve.

According to BCS theory, we can convert $T_c \sim 0.96$ K to superconducting gap $\Delta(0)$ and Pippard's coherence length ξ_0 via $\Delta(0) = 1.76 k_B T_c$ and $\xi_0 = \frac{\hbar v_F}{\pi \Delta(0)}$. Using v_F (Fermi velocity) taken from ARPES measurement, $\Delta(0)$ and ξ_0 can be estimated as 0.15 meV and 1500 nm, respectively. One can also estimate the mean free path $l = \frac{1}{k_F} \cdot \frac{h/e^2}{R_n}$ of this system using Fermi wavelength obtained by ARPES, resulting in $l = 2.4$ Å. This is much shorter than $\xi_0 = 1500$ nm, meaning that the present system can be regarded as a dirty superconductor. Effective coherence length ξ in a dirty limit superconductor is estimated as $\xi = 0.85\sqrt{\xi_0 l} = 16$ (nm). At a dirty limit, BKT transition temperature can also be estimated by [52]

$$\frac{T_{BKT}}{T_c} \sim \frac{1}{1 + 0.17\frac{R_n}{\hbar/e^2}}. \tag{5}$$

$T_{BKT} = 0.73$ K obtained from equation (5) is in a good agreement with $T_{BKT} = 0.80 \pm 0.05$ K estimated from the Halperin–Nelson fitting above. This confirms that the present system shows BKT transition as a dirty-limit superconductor.

Figures 5(a) and (b) show the sheet resistivities of 6 × 6-Tl as a function of temperature measured at different values of perpendicular magnetic field. In particular, figure 5(a) represents the high-resistance region of 7.0–8.8 kΩ. Except for 1.00 T, each curve has onset of superconductivity where the sign of $\mathrm{d}R/\mathrm{d}T$ changes from negative to positive (denoted by the black dotted line in figure 5(a)). Raising of the magnetic field decreases the onsets and eventually, at the fields larger than 0.4 T, resistivity rises with decreasing temperature toward the lowest temperature, i.e. showing insulating behavior in the zero temperature limit. This suggests the presence of magnetic-field-induced SIT (B-SIT).

Furthermore, we found another phase transition in the superconducting side under finite magnetic field. As one can see in figure 5(b), which focuses on the region below 8 kΩ, resistances drop gradually with cooling. This can be interpreted as the amplitude fluctuations, which affect superconducting properties even in the presence of magnetic field [53]. In this region, $\mathrm{d}^2R/\mathrm{d}T^2 < 0$, that is, the resistance drop is accelerated as lowering the temperature. Once across the boundary denoted by the black dotted line in figure 5(b), however, $\mathrm{d}^2R/\mathrm{d}T^2$ becomes positive, i.e, $R - T$ curves saturate toward the lowest temperature with finite residual resistivities. These plateau suggest the presence of an intermediate 'metallic state', which has finite resistivity. For understanding this non-trivial temperature dependence under finite magnetic field, we performed numerical fittings with theoretical models describing dissipative vortices motion in the $R(T,B)$ behaviors. In usual cases of broaden superconducting transitions due to magnetic field, vortices should be driven by thermal activation (thermally activated flux flow, TAFF), causing the dissipation written as $R \propto \exp\left(\frac{-U(B)}{k_B T}\right)$, where $U(B)$ is the activation energy [54]. Figure 5(c) shows Arrhenius plot for fixed magnetic fields in semilog scale. Even though TAFF is widely observed in 2DSC, $R(1/T)$ curves of the the 6 × 6-Tl deviate from $R \propto \exp(1/T)$. As we have seen above, amplitude fluctuations are dominant for higher temperatures. For lower temperatures, the resistance saturates to a level dependent on the magnetic field, thus indicating transition into the quantum metallic state.

A possible picture of the intermediate metallic state between the superconductor and insulator is the Bose metal (BM) [14, 55–59]. In the model, a 2D system of interacting bosons may form a gapless, nonsuperfluid state in the limit of zero temperature. It is argued that the uncondensed Cooper pairs and vortices cause the small resistance even under small finite field. A magnetic field is responsible for gauge fluctuations, which disrupt phase coherence and cause dissipation. The induced resistance which is proportional to the free (anti) vortices density n_v as $R \propto R_Q n_v \mu_v$. Here, μ_v is vortex mobility. n_v scales as $n_v \sim 1/\xi_+^2$. ξ_+ is superfluidicity correlation length which diverges across the boundary of superconductor-BM transition with an exponent ν_0, i.e. $\xi_+ \sim (B - B_{c0})^{-\nu_0}$ where B_{c0} is the critical field of the superconductor to BM state. As a result, resistivity across the field-tuned transition from superconductor to metallic state is described by [56]

$$R \propto (B - B_{c0})^{2\nu_0}. \qquad (6)$$

Figure 5(d) shows a log–log plot of sheet resistivities versus magnetic field taken at several different temperatures. The curve at 0.85 K obeys a power-law dependence on the magnetic field. We have fitted the data to equation (6). In figure 5(d), solid black line represents the fitting result, which shows excellent agreement with the data at $T = 0.85$ K. This yields the critical exponent of $\nu_0 = 0.60$. In other experimental examples employing this analysis, $\nu_0 \sim 0.5$ [59] and $\nu_0 = 1.61$ [14] were reported in the MoGe thin film and exfoliated $NbSe_2$ thin flake, respectively. The numerical fitting also gives us the critical field of $B_{c0} \sim 0$ T, suggesting that the system is in the metallic phase at 0.85 K even without magnetic field. This is reasonable since, under zero magnetic field, a zero-resistivity state survives below 0.8 K due to vortex-antivortex generation as discussed above.

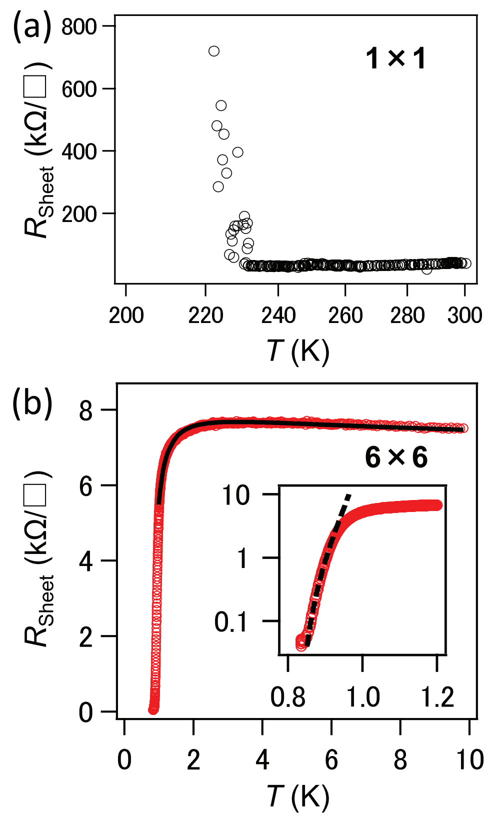

Figure 4. Sheet resistivities as a function of temperature. (a) Single-layer 1 × 1-Tl surface. It shows abrupt uprise at 230 K. (b) Double-layer 6 × 6-Tl surface. Resisitivity starts to drop at around 4 K, and reaches zero below 1 K. The black solid line represents a result of the least-squares fit to conductivity including Aslamazov–Larkin term and ln T components (equation (1)). Inset shows the resistive transition plotted in a semilogarithmic scale. The black dashed line represents the Berezinskii–Kosterlitz–Thouless transition using the Halperin–Nelson equation (equation (4)). This yields superconducting and BKT transition temperatures $T_c = 1.0$ K and $T_{BKT} = 0.80$ K, respectively.

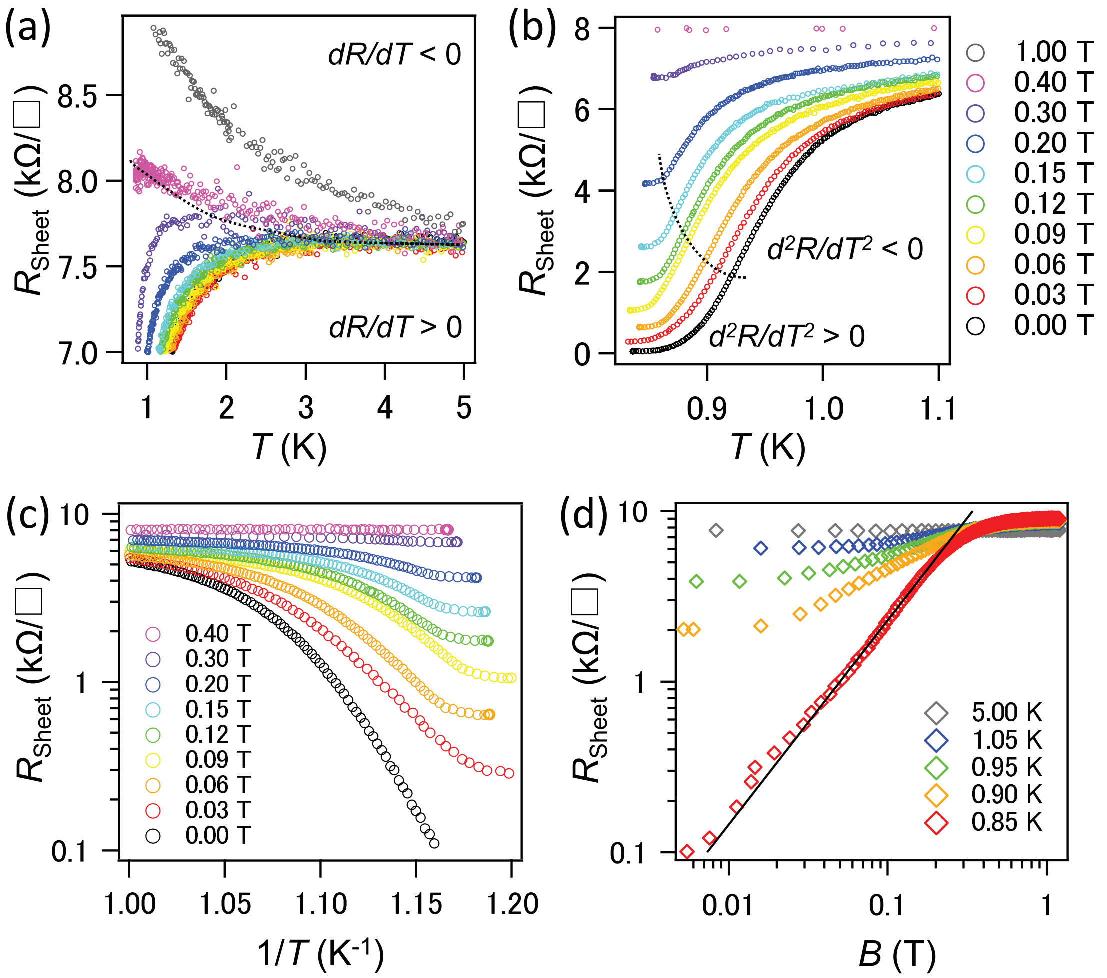

Figure 5. Sheet resistivities under different magnetic fields applied perpendicular to the surface. (a) Temperature dependencies in the high-resistance region (7.0–8.8 kΩ). A black dotted line indicates the boundary where the sign of dR/dT changes, namely, superconductor-insulator transition occurs. (b) Same in the low-resistance region (0–8 kΩ). Black dotted line indicates the boundary where the sign of d^2R/dT^2 changes. (c) Arrhenius plots of resistance for several magnetic fields showing the vanishing of the thermally activated regime. (d) Magnetoresistance for different temperatures. The curve obtained at 0.85 K is empirically fitted by the scaling function of superconductor-Bose metal transition (black solid line).

While all of the characteristics suggest the presence of the Bose-metal-like intermediate state at low temperature, the system undergoes usual SIT for higher temperature [56, 59]. The transition field of B-SIT (B_c) should appear as a crossing point of $R - B$ curves measured at various temperatures [10, 60–63]. Figure 5(d) shows clearly an existence of a critical value of the magnetic field, $B_c = 0.39$ T, at which $R_{\text{sheet}} = R_c = 8.0$ kΩ is independent of the temperature.

Close to the SI transition, i.e. at $B = B_c$ and $T = 0$, the linear response and the nonlinear response of the system are governed by the divergence of the correlation length ξ [53]. In the critical regime, the divergence of ξ is cut off by a length scale l_T, which is determined by the temperature as $l_T \sim T^{-1/z}$. One can derive a scaling relation for R_{sheet} with temperature and magnetic field near B_c:

$$R(B, T) = F\left(\frac{|B - B_c|}{T^{z\nu}}\right), \tag{7}$$

where $F\left(\frac{|B - B_c|}{T^{z\nu}}\right)$ is an arbitrary scaling function. Scaling of the zero bias resistance with T and B determines the product $z\nu$. We plotted $R_{\text{sheet}}(B, T)$ against the scaling variable $\frac{|B - B_c|}{T^{z\nu}}$, and adjust the power $z\nu$ to obtain the best visual coincidence of the data [53] except for the very low temperatures, where resistance saturates to a magnetic-field-dependent level. Figure 6(a) shows the splitting of $R_{\text{sheet}}(B, T)$ into two branches, assuming $z\nu = 0.2$. Generally speaking, the value of $z\nu$ relates to universality class of the system. For example, $z\nu = 4/3$ or $2/3$ correspond to the classical percolation and the 3D XY models, respectively. $z\nu = 0.2$ deviates from these typical examples. $z\nu$ larger than 4/3 have been found in ultrathinned cuprate systems [64–66]. Furthermore, temperature-dependent $z\nu$ have recently been reported for the epitaxial two-dimensional systems [8, 10]. In these studies, $z\nu$ grows rapidly with decreasing temperature and tends to diverge with the field approaching a critical value. This divergence is regarded as quantum Griffiths singularity, where the dynamical exponent z obeys activated scaling behavior. The quantum Griffiths singularity indicates that the system is under the domination of quenched disorder, i.e. time-independent random potentials such as

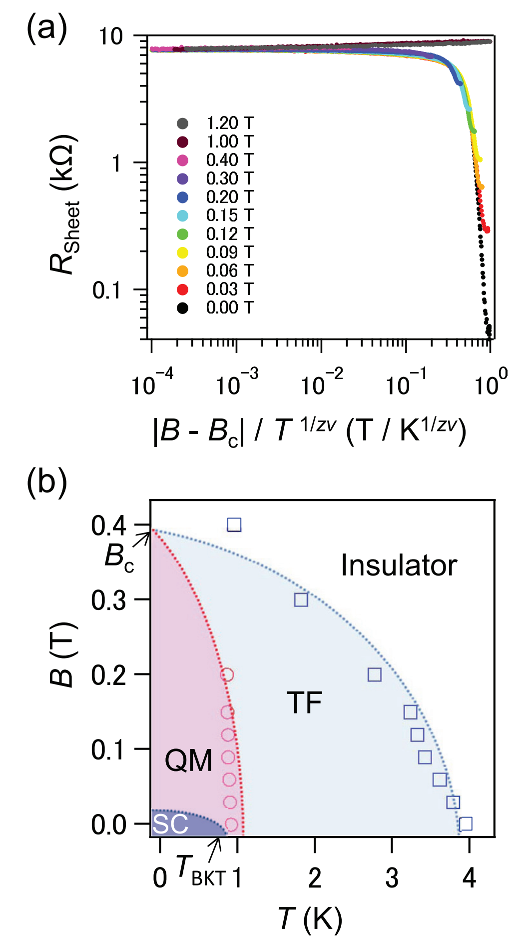

Figure 6. (a) The result of usual scaling analysis of SIT: all data of the sheet resistance shown in figure 5 are summarized as a function of the scaling variable $|B - B_c|/T^{1/z\nu}$. (b) Full $B - T$ phase diagram of the Tl double layer. The blue squres denotes the phase boundary of superconductor-insulator transition, where the sign of dR/dT changes (the black dotted line in figure 5(a)). The red circles, dividing the quantum metal (QM) state from a state dominated by strong thermal fluctuation (TF) of order parameter, mark the transition where d^2R/dT^2 changes their sign (the black dotted line in figure 5(b)).

vacancies, defects and impurity atoms. The temperature dependence originates from the interplay of quenched disorder and thermal/quantum fluctuations. As seen in figure 1, the superconducting double layer of Tl has not only atomic defects or steps, but also spatial fluctuations of coverage. The bare 1×1 single Tl layer area is an insulator that should act as Josephson junction between areas of the superconducting 6×6-Tl double layer. This structure is consistent with the situation where quantum Griffiths singularity occurs. However, it is hidden by strong thermal fluctuations because at the temperature range where the scaling equation (7) is applied, thermal fluctuations are dominant as seen in figure 5(b). Thus, this region corresponds to *the high-temperature phase* of quench-disordered system. Despite the presence of disorder, the high-temperature phase should be regarded as a clean system, where ν is determined by the Harris criterion. The Harris criterion suppresses ν as $d\nu < 2$, where d is dimension, leading to small value of $z\nu$, for example, 0.32 in [10]. For the lower temperatures, vortex glass state is expected to be induced by magnetic field due to a quenched disorder. In the vortex glass phase, variable range of hopping (VRH) of vortices generates finite resistance: $R \propto \exp[-(T_0/T)^{1/3}]$ [67, 68]. $R - T$ curves of the 6×6-Tl under magnetic field are not consistent with this relation due to saturation of resistance at very low temperatures. In this sense, as described above, Bose metal is the most plausible picture to produce metallic state in the 6×6-Tl double layer.

A phase diagram of the present system is presented in figure 6(b). The phase transition at high temperature and field is described by usual scaling analysis of SIT. Its boundary is determined by the black dotted line in figure 5(a) and shown as squares with guideline in figure 6(b). However, the present system does not transfer directly into the pure superconducting state. First, Cooper pair formation is governed by thermal fluctuations, which generate the gradual decreasing of resistivity. Decreasing of resistivity is accelerated by mean-field superconductivity. However, global phase coherence is suppressed by gauge fluctuations. The system turns into quantum metallic state (the boundary is shown by the black dotted line in figure 5(b) and as circles with guideline in figure 6(b)), where bosonic Cooper pairs are spatially confined by the localization length of randomly induced strong phase fluctuations. In other words, dissipation of unbinded vortex-antivortex pairs causes finite resistivity that survives even at zero-magnetic field. True superconductivity, namely, zero resistance state is achieved by binding of the vortex-antivortex pairs at T_{BKT} according to BKT scenario. It should be noted that Dalidovich and Phillips pointed out that Bose metal state is a 'phase glass' where superconductor loses global phase coherence [57, 58]. Although vortex and phase glasses are not identical, there remains room for discussion about correlation of these two states.

Conclusion

Thallium adsorption on the Si(1 1 1)-1×1-Tl surface at ambient temperature results in the formation of 'soft' incommensurate 6×6-Tl double-layer film on the entire surface of sample which has a metallic character in contrast to the single-layer 1×1-Tl insulating surface. This finding of growth condition enables us to measure the resistance by four-point probe method. The 6×6-Tl double layer exhibits superconducting transition at 0.96 K. The transition is broaden by amplitude and phase fluctuations of order parameter, which are described by Aslamazov–Larkin and Halperin–Nelson formulas, respectively. By applying perpendicular magnetic field, we found a magnetic field induced superconductor-insulator transition (SIT). At the high-temperature regime, the data show good agreement with the usual scaling law of SIT. Obtained small value of $z\nu = 0.2$ implies that the present system is in the high-temperature phase of 2DSC with a quenched disorder. At the lower-temperature regime, we observed an intervening metallic state. Magnetoresistive measurement close to the lowest temperature suggests that the intermediate state is a Bose metal, generated by gauge fluctuations due to magnetic field. This is an extension of phase fluctuation effect without magnetic field, namely, BKT physics.

These superconducting characteristics strongly suggest the intrinsic two-dimensionality of the present system. This in return proves the advantage of epitaxially grown metallic overlayers on semiconductor surfaces as platforms to investigate 2DSC using surface analysing techniques. For example, further adsorption of various kinds of atoms/molecules, which creates disorder or career transfer, should modify 2DSC properties. Such local-structure-derived superconducting properties can be more directly investigated by ultralow-temperature STM/S. This is promising to study not only the bosonic nature under magnetic field but also microscopic origin of superconductivity, e.g. pairing symmetry of Cooper pairs. Application of in-plane magnetic field to 2DSC is more interesting since orbital breaking of Cooper pairs is prohibited. Then, the upper critical field is determined by the paramagnetic effect, which is strongly affected by spin-orbit coupling. For instance, gate-induced 2DES in MoS_2 shows a huge upper critical field due to Cooper pair formation between spin-polarized valleys [69]. In this sence, a hybrid structure 1×1- and 6×6-Tl on Si(1 1 1) is promising since the former reconstruction has spin-polarized valleys and the latter can append superconductivity in it by proximity effect.

Acknowledgments

We thank T Hashimoto, A Takayama, R Akiyama, and R Hobara for their useful discussion and assistance in experiments. This work was supported by the JSPS (KAKENHI 15H02105, 16H02108, 25246025, 22246006), the MEXT (Grant-in-Aid for Scientific Research on Innovative Areas 'Molecular Architectonics' 25110010) and Russian Foundation for Basic Research (Grant 16-52-50049). SI thanks JSPS for financial support.

References

[1] Haviland D, Liu Y and Goldman A 1989 *Phys. Rev. Lett.* **62** 2180
[2] Goldman A M and Marković N 1998 *Phys. Today* **51** 39
[3] Clem J R 1991 *Phys. Rev.* B **43** 7837
[4] Ueno K, Nakamura S, Shimotani H, Ohtomo A, Kimura N, Nojima T, Aoki H, Iwasa Y and Kawasaki M 2008 *Nat. Mater.* **7** 855
[5] Saito Y, Kasahara Y, Ye J, Iwasa Y and Nojima T 2015 *Science* **350** 409
[6] Reyren N *et al* 2007 *Science* **317** 1196
[7] Reyren N, Gariglio S, Caviglia A, Jaccard D, Schneider T and Triscone J 2009 *Appl. Phys. Lett.* **94** 112506
[8] Shen S *et al* 2016 *Phys. Rev.* B **94** 144517
[9] Zhang H-M *et al* 2015 *Phys. Rev. Lett.* **114** 107003
[10] Xing Y *et al* 2015 *Science* **350** 542
[11] Ge J F, Liu Z L, Liu C, Gao C L, Qian D, Xue Q K, Liu Y and Jia J F 2015 *Nat. Mater.* **14** 285
[12] Ludbrook B *et al* 2015 *Proc. Natl Acad. Sci.* **112** 11795
[13] Ichinokura S, Sugawara K, Takayama A, Takahashi T and Hasegawa S 2016 *ACS Nano* **10** 2761
[14] Tsen A W, Hunt B, Kim Y D, Yuan Z, Jia S, Cava R J, Hone J, Kim P, Dean C R and Pasupathy A N 2015 *Nat. Phys.* **12** 208
[15] Xi X, Wang Z, Zhao W, Park J H, Law K T, Berger H, Forró L, Shan J and Mak K F 2015 *Nat. Phys.* **12** 139
[16] Anderson M, Ensher J, Matthews M, Wieman C and Cornell E 1995 *Science* **269** 198
[17] Greiner M, Mandel O, Esslinger T, Hänsch T W and Bloch I 2002 *Nature* **415** 39
[18] Zhang T *et al* 2010 *Nat. Phys.* **6** 104
[19] Uchihashi T, Mishra P, Aono M and Nakayama T 2011 *Phys. Rev. Lett.* **107** 207001
[20] Yamada M, Hirahara T and Hasegawa S 2013 *Phys. Rev. Lett.* **110** 237001
[21] Imamura T, Okamoto K, Saito M and Ohtsuka M 1976 *J. Phys. Soc. Japan* **40** 1256
[22] Vitali L, Ramsey M G and Netzer F P 1999 *Phys. Rev. Lett.* **83** 316
[23] Vitali L, Leisenberger F P, Ramsey M G and Netzer F P 1999 *J. Vac. Sci. Technol.* A **17** 1676
[24] Zotov A V, Saranin A A, Kotlyar V G, Utas O A and Wang Y L 2006 *Surf. Sci.* **600** 1936
[25] Kocán P, Visikovskiy A V, Ohira Y, Yoshimura M, Ueda K and Tochihara H 2008 *Appl. Surf. Sci.* **254** 7647
[26] Kim N D, Hwang C G, Chung J W, Kim Y, Kim T C, Noh D Y, Sumitani K, Tajiri H and Sakata O 2008 *Surf. Sci.* **602** 369
[27] Lee G, Hwang C G, Kim N D, Chung J and Kim J S 2007 *Phys. Rev.* B **76** 245409
[28] Hwang C G, Kim N D, Lee G, Shin S Y, Kim J S and Chung J W 2008 *New J. Phys.* **10** 053013
[29] Kotlyar V G, Saranin A A, Zotov A V and Kasyanova T V 2003 *Surf. Sci.* **543** L663
[30] Özkaya S, Çakmak M and Alkan B 2008 *Surf. Sci.* **602** 1376
[31] Özkaya S, Çakmak M and Alkan B 2014 *Phys. Status Solidi* B **251** 1570
[32] Vitali L, Ramsey M G and Netzer F P 2001 *Appl. Surf. Sci.* **175–6** 146
[33] Kocán P, Sobotík P and Ošt'ádal I 2011 *Phys. Rev.* B **84** 233304
[34] Lee S S, Song H J, Kim N D, Chung J W, Kong K, Ahn D, Yi H, Yu B D and Tochihara H 2002 *Phys. Rev.* B **66** 233312
[35] Noda T, Mizuno S, Chung J and Tochihara H 2003 *Japan. J. Appl. Phys.* **42** L319
[36] Kim N D, Hwang C G, Chung J W, Kim T C, Kim H J and Noh D Y 2004 *Phys. Rev.* B **69** 195311
[37] Sakamoto K *et al* 2009 *Phys. Rev. Lett.* **102** 096805
[38] Ibañez-Azpiroz J, Eiguren A and Bergara A 2011 *Phys. Rev.* B **84** 125435
[39] Sakamoto K *et al* 2013 *Nat. Commun.* **4** 2073
[40] Stolwijk S D, Schmidt A B, Donath M, Sakamoto K and Krüger P 2013 *Phys. Rev. Lett.* **111** 176402
[41] Stolwijk S D, Sakamoto K, Schmidt A B, Krüger P and Donath M 2014 *Phys. Rev.* B **90** 161109
[42] Nakajin K and Murakami S 2015 *Phys. Rev.* B **91** 245428
[43] Stolwijk S D, Sakamoto K, Schmidt A B, Krüger P and Donath M 2015 *Phys. Rev.* B **91** 245420
[44] Vitali L, Ramsey M G and Netzer F P 2000 *Surf. Sci.* **452** L281
[45] Kraft J, Surnev S L and Netzer F P 1995 *Surf. Sci.* **340** 36
[46] Park J W and Kang M H 2012 *Phys. Rev. Lett.* **109** 166102
[47] Uchida K and Oshiyama A 2013 *Phys. Rev.* B **87** 165433
[48] Matetskiy A V, Ichinokura S, Bondarenko L V, Tupchaya A Y, Gruznev D V, Zotov A V, Saranin A A, Hobara R, Takayama A and Hasegawa S 2015 *Phys. Rev. Lett.* **115** 147003
[49] Yamada M, Hirahara T, Hobara R, Hasegawa S, Mizuno H, Miyatake Y and Nagamura T 2012 *e-J. Surf. Sci. Nanotechnol.* **10** 400
[50] Larkin A and Varlamov A 2005 *Theory of Fluctuations in Superconductors* (Oxford: Clarendon)
[51] Halperin B and Nelson D R 1979 *J. Low Temp. Phys.* **36** 599
[52] Epstein K, Goldman A and Kadin A 1982 *Phys. Rev.* B **26** 3950
[53] Gantmakher V F and Dolgopolov V T 2010 *Phys.—Usp.* **53** 1
[54] Takano T, Kasahara Y, Oguchi T, Hase I, Taguchi Y and Iwasa Y 2011 *J. Phys. Soc. Japan* **80** 023702
[55] Das D and Doniach S 1999 *Phys. Rev.* B **60** 1261
[56] Das D and Doniach S 2001 *Phys. Rev.* B **64** 134511
[57] Dalidovich D and Phillips P 2002 *Phys. Rev. Lett.* **89** 027001

[58] Phillips P and Dalidovich D 2003 *Science* **302** 243
[59] Mason N and Kapitulnik A 2001 *Phys. Rev.* B **64** 060504
[60] Hebard A and Paalanen M 1990 *Phys. Rev. Lett.* **65** 927
[61] Sambandamurthy G, Engel L, Johansson A and Shahar D 2004 *Phys. Rev. Lett.* **92** 107005
[62] Baturina T I, Islamov D R, Bentner J, Strunk C, Baklanov M and Satta A 2004 *J. Exp. Theor. Phys. Lett.* **79** 337
[63] Qin Y, Vicente C L and Yoon J 2006 *Phys. Rev.* B **73** 100505
[64] Bollinger A T, Dubuis G, Yoon J, Pavuna D, Misewich J and Božović I 2011 *Nature* **472** 458
[65] Leng X, Garcia-Barriocanal J, Bose S, Lee Y and Goldman A 2011 *Phys. Rev. Lett.* **107** 027001
[66] Zeng S *et al* 2015 *Phys. Rev.* B **92** 020503
[67] Auerbach A, Arovas D P and Ghosh S 2006 *Phys. Rev.* B **74** 064511
[68] Koren G, Mor Y, Auerbach A and Polturak E 2007 *Phys. Rev.* B **76** 134516
[69] Saito Y *et al* 2015 *Nat. Phys.* **12** 144